THE JOURNAL OF BIOLOGICAL CHEMISTRY VOL. 284, NO. 24, pp. 16621–16632, June 12, 2009

Cyclin D3 Mediates Synthesis of a Hyaluronan Matrix That Is Adhesive for Monocytes in Mesangial Cells Stimulated to Divide in Hyperglycemic Medium*[S]

Received for publication, August 19, 2008, and in revised form, March 6, 2009 Published, JBC Papers in Press, March 9, 2009, DOI 10.1074/jbc.M806430200

Juan Ren, Vincent C. Hascall, and Aimin Wang[1]

From the Department of Biomedical Engineering, Cleveland Clinic, Cleveland, Ohio 44195

Serum-starved, growth-arrested, near confluent rat mesangial cell cultures were stimulated to divide in medium with low (5.6 mM) or high (25.6 mM) glucose. In high glucose cultures Western blots showed large increases in cyclin D3 and CCAAT/enhancer-binding protein α (C/EBPα) at 48–72 h, concurrent with the production of a monocyte-adhesive hyaluronan matrix, whereas low glucose and mannitol osmotic control cultures did not. Cyclin D3 small interfering RNA inhibited both the synthesis of this matrix and the up-regulation of C/EBPα in cultures exposed to high glucose, indicating that cyclin D3 is a key mediator in regulating responses of dividing mesangial cells to hyperglycemia. A complex with cyclin D3, cyclin-dependent kinase 4, and C/EBPα was observed at 48–72 h in the hyperglycemic cultures, and cyclin D3 and C/EBPα were spatially co-localized in coalesced perinuclear honeycomb-like structures with embedded hyaluronan. Furthermore, microtubule-associated protein 1 light chain 3, a marker for autophagy, colocalizes with these structures. These results suggest that cyclin D3 is a central coordinator that controls the organization of a complex set of proteins that regulate autophagy, formation of the monocyte-adhesive hyaluronan matrix, and C/EBPα-mediated lipogenesis. Abnormal deposits of hyaluronan, cyclin D3, and C/EBPα were present in glomeruli of kidney sections from hyperglycemic rats 4 weeks after streptozotocin treatment, indicating that similar processes likely occur *in vivo*. Mesangial cell cultures treated with poly(I:C) or tunicamycin in normal glucose media synthesized monocyte-adhesive hyaluronan matrices but with concurrent down-regulation of cyclin D3. This indicates that the cyclin D3 mechanism is induced by hyperglycemia and is distinct from those involved in these cell stress responses.

One of the abnormalities detected after the onset of hyperglycemic diabetes in the streptozotocin rat model is an early (already by 3 days) and self-limited proliferation of glomerular mesangial cells that is associated with *de novo* expression of α-smooth muscle actin, an activation marker of the proliferative mesangial cell phenotype (1–3). After this early transient proliferation and phenotypic activation, there is a prominent glomerular infiltration of monocytes and macrophages (3). Our previous study showed that abnormal hyaluronan matrices also form in the hyperglycemic glomeruli within 1 week (4). We also showed that quiescent, growth-arrested rat mesangial cells, stimulated to divide in a hyperglycemic level of glucose (25.6 mM), form a hyaluronan matrix that is adhesive for U937 monocytic cells. These results suggest that there is an important link *in vivo* between mesangial cell division in response to hyperglycemia, glomerular hyaluronan matrix synthesis, and the accumulation of monocytes/macrophages in glomerular diabetic nephritis.

Previous studies have shown that smooth muscle cell cultures exposed to tunicamycin (endoplasmic reticulum stress) or poly(I:C) (viral mimetic) synthesize hyaluronan cable-like structures that are adhesive for monocytes (5, 6). The experiments described in this report indicate that growth-arrested mesangial cells stimulated to divide in hyperglycemic medium synthesize similar structures by a distinctly different mechanism that requires protein kinase C up-regulation at the initiation of cell division and subsequent up-regulation of cyclin D3 after completion of cell division. The up-regulation of cyclin D3 in turn appears to control an autophagic response and is coordinate with up-regulation of C/EBPα, a factor that controls lipogenic responses. Evidence is also provided that cyclin D3 and C/EBPα also contribute to glomerular responses to hyperglycemia *in vivo*.

EXPERIMENTAL PROCEDURES

Reagents—Streptomyces hyaluronidase, Streptococcal hyaluronidase, and chondroitinase ABC were from Seikagaku America, Inc. (Rockville, MD). Antibodies against cyclin D3 and CDK2 were from BD Biosciences. Anti-CDK4 (clone DCS-31) and anti-CDK6 antibodies (clone DCS-90) were from Sigma-Aldrich. Antibodies against C/EBPα and -β and microtubule-associated protein 1 light chain 3 (LC3)[2] were from Santa Cruz Biotechnologies (Santa Cruz, CA). Control RNA, siRNA, and siRNA transfection reagent, siPORT NeoFX, were from Ambion (Austin, TX). The siRNA sequence targeting for rat cyclin D3 is GGGUUUAAUAGGGAUGGAUtt. Cell lysis buffer for immunoprecipitation was from Pierce (catalog no. 78501).

* This work was supported, in whole or in part, by National Institutes of Health Grants R01 DK62934 (to A. W.) and 1P30 AR-050953.

[S] The on-line version of this article (available at http://www.jbc.org) contains supplemental Movies Fig. 9*A* and Fig. 9*B*.

[1] To whom correspondence should be addressed: Lerner Research Institute, ND20, Dept. of Biomedical Engineering, Cleveland Clinic, Cleveland, OH 44195. Tel.: 216-445-3237; Fax: 216-444-9198; E-mail: wanga@ccf.org.

[2] The abbreviations used are: LC3, microtubule-associated protein 1 light chain 3; C/EBP, CCAAT/enhancer-binding proteins; CDK, cyclin-dependent kinase; RMC, rat mesangial cell; FBS, fetal bovine serum; poly(I:C), a synthetic double-stranded RNA; TRITC, tetramethylrhodamine isothiocyanate; siRNA, small interfering RNA; ER, endoplasmic reticulum.

Establishment of RMC Cultures and Induction of Diabetes in Rats—RMC cultures were established from isolated glomeruli and characterized as described previously (7, 8). RMCs were used between passages 5 and 15, when they still contract in response to angiotensin II and endothelin, and they exhibit growth suppression in the presence of heparin (1 μg/ml), which are additional characteristics of mesangial cells (9–11). RMCs were cultured in RPMI 1640 medium containing 10% fetal bovine serum (FBS) and passaged at confluence by trypsinization for 5 min with a solution of 0.025% trypsin, 0.5 mM EDTA. To render cells quiescent (11), cultures at 40% confluence (2×10^4 cells/cm^2) were washed with RPMI 1640 medium and placed in fresh medium containing 0.4% FBS for 48 h (yielding 70–80% confluent cultures).

Hyperglycemic diabetes was induced in ~175-g male Sprague-Dawley rats using tail vein injections of 55 mg/kg streptozotocin (3, 12). All animals were fed standard laboratory diet. Blood was collected by tail-bleeding at day 3 after injection, and the blood glucose concentration was determined by using fluorophore-assisted carbohydrate electrophoresis analyses to confirm the onset of diabetes. After 4 weeks the kidneys were collected from both control and diabetic rats and fixed in 4% paraformaldehyde in phosphate-buffered saline at 4 °C overnight for subsequent cryo-embedding and sectioning for histological analyses (Histology Core Facility, Department of Biomedical Engineering, Cleveland Clinic).

Cell Transfection of siRNAs—RMCs were transfected with siRNA using siPORT NeoFX as the transfection reagent (Silencer^{TM} siRNA transfection kit) according to the protocol provided by Ambion. Cells were incubated with cyclin D3 siRNA (50 pmol), siRNA containing scrambled sequences (50 pmol), or no siRNA for 16 h in medium with 5.6 mM glucose and 20% FBS and then starved for 48 h in the same medium with 0.5% FBS. Medium containing 10% FBS and either 5.6 or 25.6 mM glucose or 20 mM mannitol with 5.6 mM glucose was then applied on RMCs for an additional time up to 72 h. Biochemical experiments and/or monocyte adhesion assays were done as described below.

Immunohistochemistry—Cryosections of kidneys and methanol-fixed RMC cultures on coverslips were stained for hyaluronan with a hyaluronan-binding protein (Seikagaku America), for cyclin D3, C/EBPα, and LC3 with antibodies, and for nuclei with 4,6-diamidino-2-phenylindole, as described previously (5, 13) or according to the manufacturer's instruction. Samples were treated with biotinylated hyaluronan-binding protein at a 1:100 dilution and with anti-cyclin D3 and/or anti C/EBPα antiserum at a 1:75 dilution, washed, and treated with fluorescein isothiocyanate-streptavidin at 1:500 dilution and/or with anti-mouse IgG TRITC and anti-rabbit IgG Cy5 antibodies at 1:200 dilution. Stained samples were mounted in VectaShield containing 4,6-diamidino-2-phenylindole (Vector Laboratories) for staining the nuclei of cells. Confocal images of the samples were obtained with a Leica TCS-NT laser-scanning confocal microscope equipped with four lasers for excitation at 351-, 488-, 561-, and 633-nm wavelengths. The same settings of confocal microscope and laser-scanning were used for both control and treated samples. The magenta signal of Cy5 was converted to green for data presentation using Adobe Photoshop CS2 software from Adobe System (San Jose, CA).

In some experiments mesangial cell cultures were fixed with 4% paraformaldehyde in phosphate-buffered saline for 30 min at room temperature and then permeabilized by treating them with 0.4% Triton X-100 for 10 min at room temperature (14). Permeabilized and control non-permeabilized cultures were then stained for hyaluronan, cyclin D3, and LC3 as described above.

Assay for Monocyte Adhesion (4, 5)—RMCs in 6-well plates were treated up to 72 h with 5–20% FBS and concentrations of 5.6 and 25.6 mM D-glucose. Mannitol at 20 mM with 5.6 mM D-glucose was used as an osmotic control. U937 cells were cultured in suspension in RPMI 1640 medium containing 5% FBS and passaged at a 1:5 ratio (2×10^5 cells/ml) every 48 h (5). Assays for monocyte adhesion were done as described previously (4, 5). After washing, the cell cultures were imaged by microscopy with a Polaroid digital camera (4), and the numbers of monocytes per culture area were counted using Image-Pro software. Each culture was equally divided into four regions, and a culture area for imaging was randomly picked in each region. *Streptomyces* hyaluronidase (1 turbidity unit/ml at 37 °C for 15 min) treatment of RMCs before monocyte incubation was used to determine the extent of the hyaluronan-mediated adhesion.

Fluorophore-assisted Carbohydrate Electrophoresis Analysis of Reducing Saccharides (15, 16)—Cell cultures were incubated with proteinase K at 250 μg/ml in 0.1 M ammonium acetate, pH 7.0, for 3 h at 60 °C (4). The reaction was terminated by heating the samples at 95 °C for 3–5 min. Glycosaminoglycans were recovered by 75% ethanol precipitation at −20 °C overnight and centrifugation. The dissolved pellets were incubated with streptococcal hyaluronidase (50 milliunit/ml) and chondroitinase ABC at 2 units/ml in 0.1 M ammonium acetate, pH 7.0, overnight at 37 °C to generate disaccharides from hyaluronan and chondroitin/dermatan sulfate. The reaction was terminated by heating the samples at 95 °C for 3–5 min. The sample digests were dried by centrifugal evaporation in microtubes and then subjected to reductive amination with 2-aminoacridone as described previously (4). At the end of the incubation, the samples were each mixed with glycerol to 20%, and 5-μl aliquots were then subjected to electrophoresis on Glyko Mono Composition gels with Mono Running buffer from ProZyme Inc. (San Leandro, CA). Running conditions were 500 V at 4 °C in a cold room for 1 h. Gels were imaged on an Ultra Lum transilluminator (365 nm). Images were captured and analyzed by using a Quantix cooled charge-coupled device camera from Roper Scientific/Photometrics and the Gel-Pro Analyzer program, Version 3.0 (Media Cybernetics), respectively. The hyaluronan contents were quantified according to the integrated intensity of signal bands and then normalized with DNA contents in the samples.

Western Blotting and Immunoprecipitation Techniques—For Western analysis, RMCs were lysed with the Laemmli sample buffer. For immunoprecipitation, cells were rinsed with ice-cold phosphate-buffered saline and lysed for 10 min in cell lysis buffer (Pierce). Lysates (~600 μl each containing an equivalent amount of total proteins) were cleared of cellular debris by centrifugation and precleared with protein-G-Sepharose beads

(Sigma-Aldrich) according to the manufacturer's instruction. The cleared cellular lysates were then subjected to immunoprecipitation with anti-cyclin D3 or anti C/EBPα antibodies, and the immune complexes were collected by incubation with 75 μl of protein-G-Sepharose beads. Total cell extracts or immunoprecipitated complexes were separated by 4–20% gradient SDS-PAGE gels and transferred to polyvinylidene difluoride membranes (Bio-Rad). After blocking overnight with 5% milk in phosphate-buffered saline containing 0.1% Tween 20 at 4 °C, the membranes were probed with the indicated antibodies and corresponding secondary antibodies and developed using enhanced chemiluminescence (ECL) reagent (Amersham Biosciences).

Statistical Analysis—The means and standard deviations were calculated in sample groups, and then one-way analysis of variance was used to compare the means of all three groups using SigmaStat software (Version 3.5, Systat Software, Chicago, IL). The unpaired Student's *t* test was used to compare the means of two groups.

RESULTS

Effect of Serum Concentration—Growth-arrested mesangial cells that are stimulated to divide in the presence 10% FBS and 25.6 mM (hyperglycemic) glucose for 72 h synthesized a hyaluronan matrix that is adhesive for U937 monocytic cells (4). To identify a minimal serum concentration that gives the maximum response for hyaluronan-mediated monocyte adhesion, growth-arrested mesangial cells were treated with high glucose in medium containing 5, 7.5, 10, 15, and 20% FBS for 72 h. Fig. 1 shows that the presence of 10% FBS increased hyaluronan content in the cell layer 50% (*lower panel*, *black bar*) relative to both the 5.6 mM glucose control cultures (*white bar*) and the 5.6 mM glucose plus 20 mM mannitol osmotic control cultures (*cross-hatched bar*). This increase in the hyaluronan matrix correlated with a specific ~2-fold increase in U937 cell adhesion compared with the control cultures (*upper panel*). FBS concentrations higher than 10% showed the same responses, whereas the responses to 25.6 mM glucose at FBS concentrations below 10% showed no significant differences from the control cultures. Because 10% FBS is required for the maximum mitogenic response of growth-arrested cells (11), the results indicate that a close association exists between mesangial cell proliferation and high glucose-induced production of the hyaluronan matrix. The following experiments used 10% FBS in the media.

Time Course of High Glucose Responses—Low serum starvation for 48 h arrests ~75% of mesangial cells at G_0/G_1 phase, and by 18 h after serum stimulation ~72% of growth-arrested cells progress to S-phase (17). To determine the correlation between cell cycle progression and the high glucose-induced responses, high glucose-induced monocyte adhesion and hyaluronan matrix production were analyzed at various times after adding 10% FBS to quiescent cultures. Fig. 2 shows the results of a time course experiment in which cultures were analyzed at 24, 48, and 72 h after stimulating growth-arrested mesangial cells in media with 10% FBS. The results at 72 h are similar to the results in Fig. 1 for media with 10% FBS, an ~50% increase in hyaluronan (*lower panel*) and in this case an ~3-fold increase in

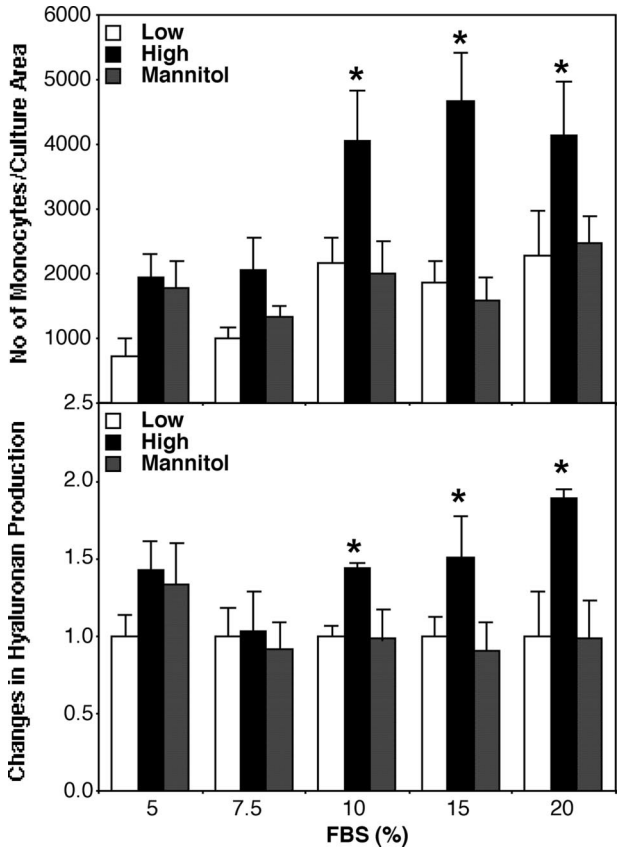

FIGURE 1. **Serum dependence of high glucose-induced monocyte adhesion and hyaluronan synthesis in cultured mesangial cells.** Serum-starved mesangial cells were stimulated with 5–20% FBS in the presence of 5.6 mM (*white bars*), or 25.6 mM (*black bars*) glucose, or 20 mM mannitol plus 5.6 mM glucose (*cross-hatch bars*) for 72 h. Monocyte adhesion (*upper panel*) and the changes in cell layer hyaluronan content (*lower panel*) were measured as described under "Experimental Procedures." The mean and S.D. were calculated from those of three duplicate experiments, and the significance of data was determined by Student's *t* test (*, $p < 0.01$, $n = 3$).

U937 cell adhesion in the presence of 25.6 mM glucose relative to the controls (*upper panel*). Statistical analysis (one-way analysis of variance) indicates that significant increases in monocyte adhesion by high glucose treatments were observed at both 48 and 72 h, compared with those of other treatments in the three test groups. Hyaluronidase digestion of mesangial cell cultures exposed to high glucose abolished the ability of the monocytes to adhere, confirming that they primarily bind directly to hyaluronan-based structures (*striped bars*). The increase in cell layer hyaluronan content in response to hyperglycemic medium is already apparent at both 24 and 48 h, but increased U937 monocyte adhesion is not apparent at 24 h. The medium containing 5.6 mM glucose with 20 mM mannitol as an osmotic control gave responses similar to ones with 5.6 mM glucose alone.

The increased hyaluronan at 24 h without monocyte adhesion suggested that the hyaluronan may be intracellular. This was demonstrated by culturing growth-arrested, preconfluent mesangial cells for 18 h in either low or high glucose media. The cultures were then stained for hyaluronan before and after exposure to 0.4% Triton X-100 to permeabilize the cells. Fig. 3 shows that the mesangial cells stimulated to divide in the high glucose medium stain extensively for hyaluronan only after Tri-

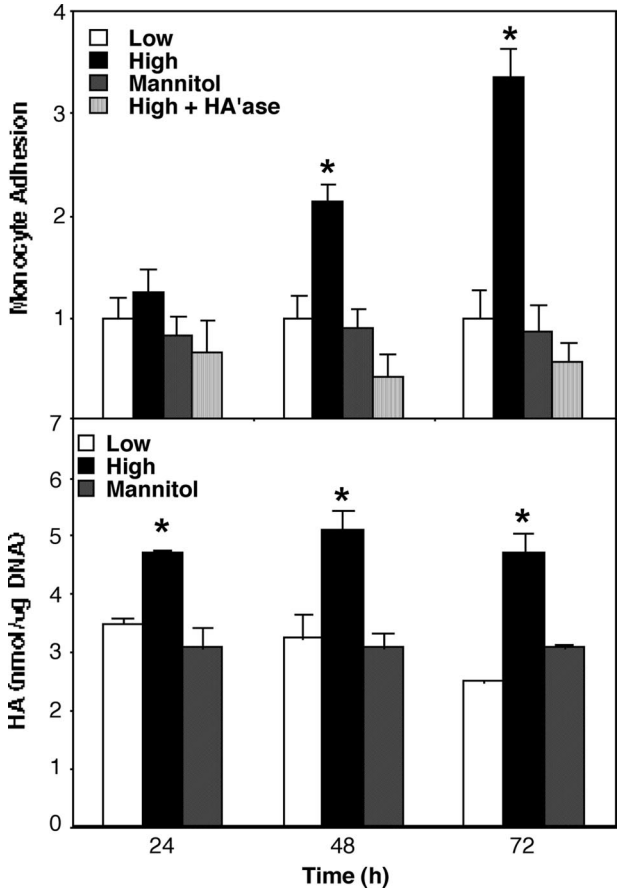

FIGURE 2. **Time course of high glucose-induced monocyte adhesion and hyaluronan synthesis in cultured mesangial cells.** Serum-starved mesangial cells were stimulated with 10% FBS in the presence of 5.6 mM (*white bars*) or 25.6 mM (*black bars*) glucose or 20 mM mannitol plus 5.6 mM glucose (*cross-hatch bars*) for 24, 48, and 72 h. *Upper panel*, the changes in monocyte adhesion by treatments of high glucose were compared with normal glucose or mannitol cultures within three groups using one-way analysis of variance test (*, $p < 0.01$, $n = 3$). The digestion of high glucose cultures with *Streptomyces* hyaluronidase (*HA'ase*, *striped bars*) confirmed the hyaluronan-mediated monocyte adhesion. *Lower panel*, the cell layer hyaluronan contents (nmol/μg DNA) in samples were quantified using the integrated intensity of hyaluronan disaccharide bands, comparing with those of hyaluronan disaccharide standard and then normalized with DNA contents. The mean values and S.D. were calculated from those of three duplicate experiments (*, $p < 0.01$, $n = 3$).

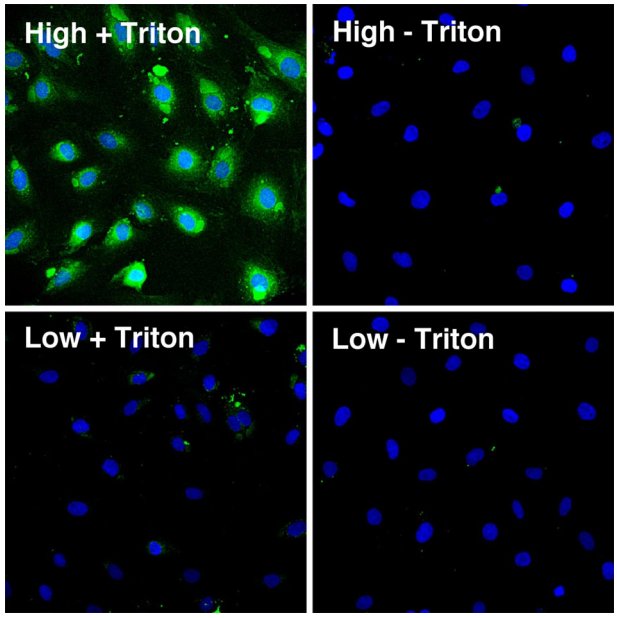

FIGURE 3. **Intracellular hyaluronan in mesangial cells stimulated to divide in hyperglycemic medium.** Serum-starved mesangial cells were stimulated with 10% FBS in the presence of 5.6 mM (*lower panels*) or 25.6 mM (*upper panels*) glucose for 18 h. Cultures were stained for hyaluronan (*green*) and nuclei (*blue*) before (*right panels*) or after (*left panels*) exposure to 0.4% Triton X-100 as described under "Experimental Procedures."

ton X-100 permeabilization. In contrast, mesangial cells stimulated to divide in low glucose medium showed little or no hyaluronan after treatment with Triton X-100.

Role of Cyclin D3 in High Glucose Responses—The results of the previous experiments indicate that re-entry into cell cycle and subsequent cell cycle progression are required for the high glucose-induced responses. To identify any cell cycle regulatory molecules involved in the high glucose-mediated responses, growth-arrested cultures were treated with 10% FBS in normal glucose, high glucose, or mannitol media. Fig. 4 shows the results of a time course in which Western blots were prepared to compare synthesis of cyclin D3 (a regulator of cell cycle progression), C/EBPα (a transcription factor that can interact with cyclin D3), C/EBPβ (a related transcription factor that does not interact with cyclin D3), and β-actin as a control. The cultures exposed to 25.6 mM glucose showed large increases in cyclin D3 and C/EBPα at 48 and 72 h compared with the low glucose and mannitol control cultures (Fig. 4*B*). In contrast, the 5.6 mM glucose control cultures and the mannitol osmotic control cultures showed no increases in C/EBPα and only modest increases in cyclin D3. None of the cultures showed significant changes in C/EBPβ. Neither cyclin D1 nor cyclin D2 showed any significant differences between cultures exposed to high and low glucose (data not shown).

Cyclin D3 forms complexes with CDK4 and/or C/EBPα to regulate cell cycle progression (18). Fig. 5 shows the results of immunoprecipitates of cyclin D3 that were then probed by Western blots for CDK4, C/EBPα, and C/EBPβ during a time course experiment. CDK4 was present at all times and for all treatments at similar levels. C/EBPα was also present in all cases but at significantly higher amounts for the 25.6 mM glucose cultures at each of the time points (*boxes*, *upper blots*). No C/EBPβ bands were observed. A reciprocal immunoprecipitation of C/EBPα was probed for cyclin D3 and also showed significantly higher amounts for the hyperglycemic cultures at all time points (*boxes*, *lower blots*). The results indicate that a high concentration of a complex with cyclin D3, CDK4, and C/EBPα is already apparent by 24 h in the hyperglycemic cultures.

To confirm the role of cyclin D3 in mediating the high glucose induced responses, cyclin D3 siRNA was used to block its synthesis. Fig. 6 shows the results of an experiment to determine the effect of cyclin D3 siRNA on the production of the hyaluronan matrix and U937 cell adhesion. Preconfluent mesangial cell cultures were treated for 16 h with reagents only, or a scramble RNA, or cyclin D3 siRNA as described under "Experimental Procedures." The cultures were then growth-arrested for 48 h in medium with 0.4% FBS. They were then stimulated to divide in medium with 10% FBS and either 5.6 mM glucose, 25.6 mM glucose, or the mannitol osmotic control. The

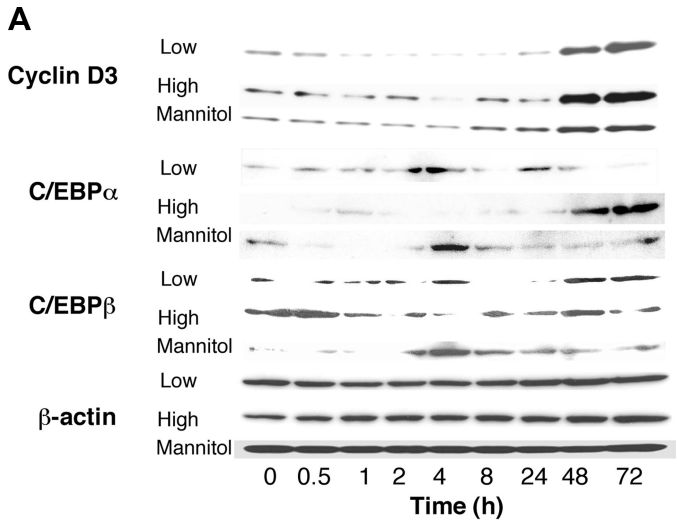

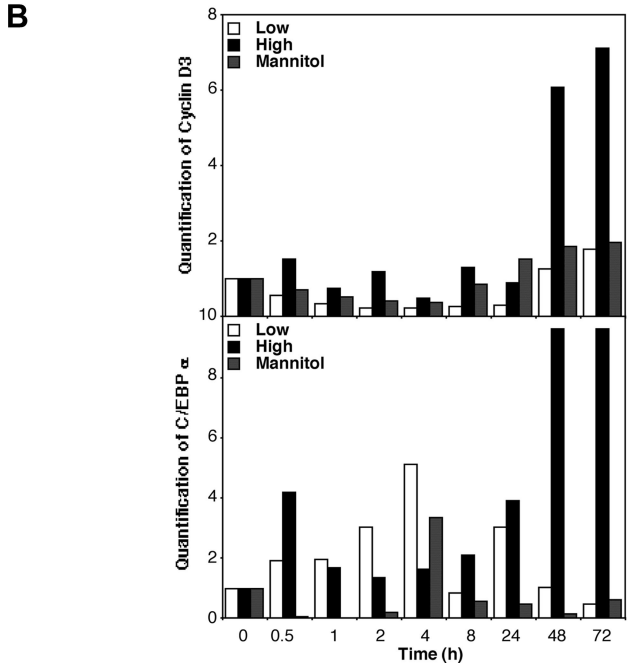

FIGURE 4. **Induction of cyclin D3 and C/EBPα by high glucose in cultured mesangial cells.** Serum-starved mesangial cells were stimulated with 10% FBS in the presence of 5.6 mM (*white bars*) or 25.6 mM (*black bars*) glucose or 20 mM mannitol plus 5.6 mM glucose (*cross-hatch bars*) for 0–72 h. Western blots were done with total cellular lysates using antibodies against cyclin D3, C/EBPα, C/EBPβ, and β-actin as described under "Experimental Procedures" (*panel A*). Protein levels of cyclin D3 and C/EBPα were calculated as ratios to β-actin and are shown in the *bar graph* (*panel B*). The data are representative of three independent experiments.

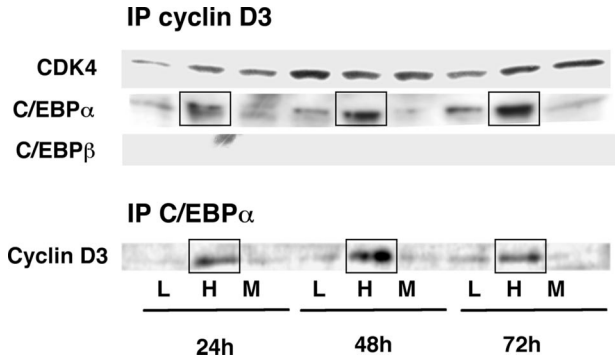

FIGURE 5. **Induction of cyclin D3 and C/EBPα complexes by high glucose in cultured mesangial cells.** Serum-starved mesangial cells were stimulated with 10% FBS in the presence of 5.6 mM (*L*) or 25.6 mM (*H*) glucose or 20 mM mannitol plus 5.6 mM glucose (*M*) for 24, 48, and 72 h. The cells were lysed, and immunoprecipitates (*IP*) of the cellular lysates with equal amounts of total proteins were done as described under "Experimental Procedures" with anti-cyclin D3 (*top panel*) or anti C/EBPα (*lower panel*) antibodies. The immunoprecipitated complexes were analyzed by Western blots with antibodies for cyclin D3, CDK4, C/EBPα, and C/EBPβ. The *boxes* highlight the responses to high glucose. The data are representative of three independent experiments.

reagent and scramble siRNA showed significant increases in hyaluronan (*lower panel*) and U937 cell adhesion (*upper panel*) at 72 h relative to the 5.6 mM glucose and mannitol control cultures. In contrast, neither hyaluronan nor U937 cell adhesion was increased in the cyclin D3 siRNA-treated cultures relative to the control cultures. Furthermore, the Western blots show significant increases in cyclin D3 and C/EBPα in cultures exposed to 25.6 mM glucose relative to those exposed to 5.6 mM glucose for both reagent and scramble RNA treatments. In contrast, both cyclin D3 and C/EBPα were inhibited to the control level in cultures exposed to 25.6 mM glucose and treated with cyclin D3 siRNA (Fig. 6*B*). These results indicate that cyclin D3 is required to induce the formation of the hyaluronan matrix that is adhesive for the U937 cells.

Fig. 7, *A–D*, shows bright-field micrographs of mesangial cell cultures analyzed for U937 cell adhesion. Monocyte adhesion to mesangial cell cultures incubated with 25.6 mM glucose was greatly increased (Fig. 7*B*) compared with cultures treated with 5.6 mM glucose or with 20 mM mannitol in 5.6 mM glucose as an osmotic control (Fig. 7, *A* and *C*). The role of cyclin D3 in the high glucose-induced hyaluronan matrix formation was underscored by showing that cyclin D3 siRNA-treated mesangial cells cultured in high glucose medium have greatly diminished monocyte adhesion (Fig. 7*D*). Fig. 7, *E–H*, shows confocal micrographs of parallel cultures stained for hyaluronan (*green*), cyclin D3 (*red*), and nuclei (*blue*). High glucose induced increases in both hyaluronan and cyclin D3 in mesangial cell cultures (Fig. 7*F*). These increases were not observed in 5.6 mM glucose- or mannitol-treated cultures (Fig. 7, *E* and *G*) and were blocked by the treatment of high glucose cultures previously treated with cyclin D3 siRNA (Fig. 7*H*), consistent with data from monocyte adhesion, fluorophore-assisted carbohydrate electrophoresis and Western analyses (Fig. 6).

Spatial Localization of Cyclin D3 and Hyaluronan Cable Structures—U937 monocytes adhere to the high glucose-induced hyaluronan structures synthesized by mesangial cells in both cluster and bead-like strand patterns (4), similar to ones observed in colon smooth muscle cells in response to viral stimuli (5). To determine spatial relationships between cyclin D3 and high glucose induced hyaluronan cable structures, mesangial cells were stained for hyaluronan, cyclin D3, C/EBPα, and nuclei 48 h after stimulating them to divide in the presence of hyperglycemic glucose. Remarkable continuous hyaluronan cable structures (*green*) were observed with closely associated, coalesced, and intertwined spots of cyclin D3 (*red*) distributed along them (Fig. 8*A*). Furthermore, Fig. 8*B* shows that C/EBPα and cyclin D3 are spatially co-localized in the coalesced structures. Note also the magnified pictures of two cells adjacent to

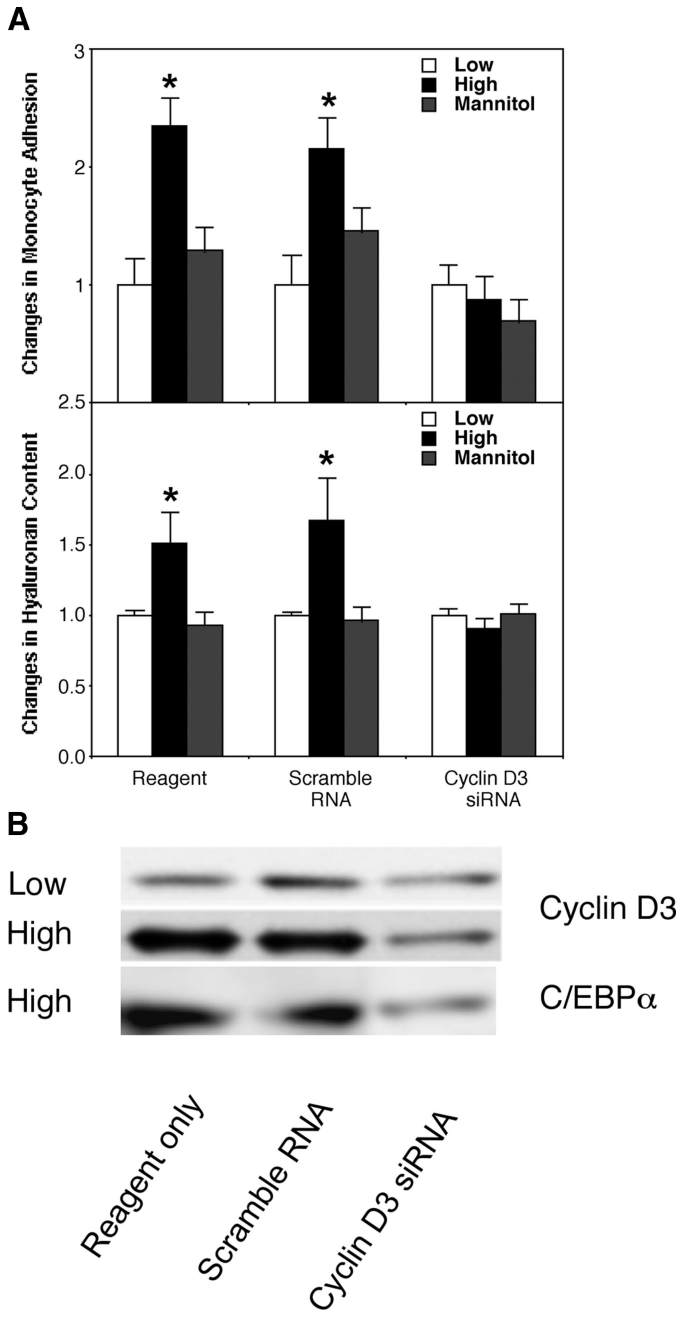

FIGURE 6. **Effect of cyclin D3 siRNA on high glucose-induced monocyte adhesion and hyaluronan synthesis.** Mesangial cells were treated for 16 h with transfect reagent alone or scramble siRNA or cyclin D3 siRNA as described under "Experimental Procedures." They were then growth-arrested for 48 h in 0.4% FBS followed by 10% FBS stimulation for 72 h in the presence of 5.6 mM (*white bars*) or 25.6 mM (*black bars*) glucose or 20 mM mannitol plus 5.6 mM glucose (*cross-hatch bars*). The changes in monocyte adhesion (*A*, *upper panel*) and cell layer hyaluronan contents (*A*, *lower panel*) by treatments of high glucose and mannitol were measured as described under "Experimental Procedures." The mean values and S.D. were calculated from those of three duplicate experiments (*, $p < 0.01$, $n = 3$). *Panel B* shows Western blots for cyclin D3 and C/EBPα from duplicate cultures.

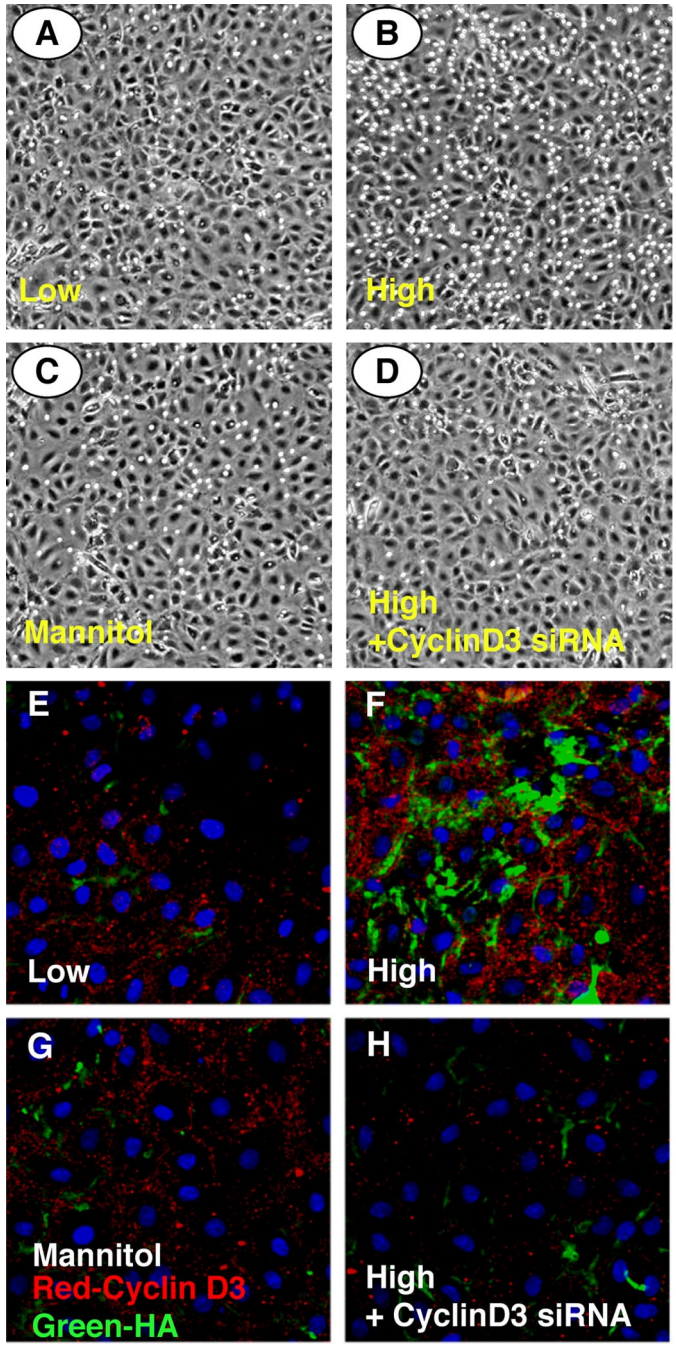

FIGURE 7. **Microscopic analyses of hyaluronan, cyclin D3 expression, and monocyte adhesion.** *Panels A–D* show bright-field images of monocyte adhesion to mesangial cell cultures prepared as described in the Fig. 5 legend with the addition of a mannitol control culture. *Panels E–H* show confocal microscopic analysis of hyaluronan and cyclin D3 in mesangial cell cultures prepared on coverslips in the same protocols as for *panels A–D*. They were then stained for hyaluronan (*green*), cyclin D3 (*red*), and nuclei (*blue*) as described under "Experimental Procedures."

the hyaluronan cable (*arrows*) and two closely associated with it (*asterisks*) in Fig. 8*C*. The *one on the left* shows clustering of cyclin D3 adjacent to the nucleus and is typical of several cells. The *adjacent panel* shows an example of clustered cyclin D3 with integrated localized hyaluronan in a "honeycomb-like" configuration. This is likely a cell that is initiating the synthesis of the hyaluronan matrix, consistent with hyaluronan synthesis initiated inside the cells (Fig. 3). The *right two panels* show cells with coalesced cyclin D3 attached to the cable structure. The *far right panel* is saturated for the hyaluronan (*green*) in the cable structure to show what appears to be vesicular structures distributed around the cyclin D3-coalesced structures and in the cell cytoplasm, similar to the patterns observed in dividing smooth muscle cells (14) and in cells undergoing autophagy

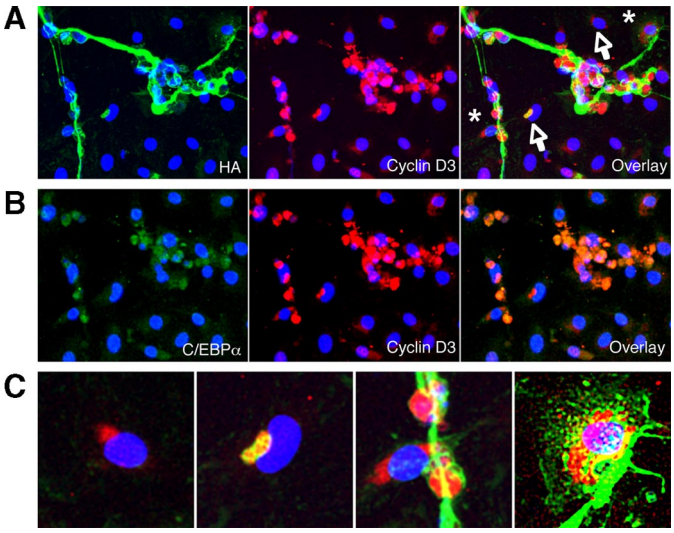

FIGURE 8. **Confocal microscopic analysis of hyaluronan cable structures, cyclin D3, and C/EBPα in high glucose-treated mesangial cells.** A mesangial cell culture on a coverslip was treated with the high glucose protocol for 48 h and then stained for hyaluronan (*HA, green*) for cyclin D3 (*red*), C/EBPα (*magenta*), and nuclei (*blue*) as described under "Experimental Procedures." Specificity of each antibody was confirmed by the absence of fluorescent signal when the primary antibody was omitted (not shown). Hyaluronan structures and the proteins were visualized under confocal microscopy. *Panel A* shows confocal microscopic images of hyaluronan structures (*green*), cyclin D3 (*red*), and nuclei (*blue*). *Panel B* shows confocal microscopic images of C/EBPα (*magenta* converted to *green*), cyclin D3 (*red*), and nuclei (*blue*) staining in the same region as in *panel A*. C/EBPα and cyclin D3 are spatially co-localized in the coalesced structures attached to the hyaluronan cables. *Panel C* shows enlarged images of two cells (*left panels*) adjacent to the hyaluronan cable structure (*arrowheads* in *panel A*) and two cells (*right panels*) closely engaged with the hyaluronan cable structure (*asterisks* in panel *A*).

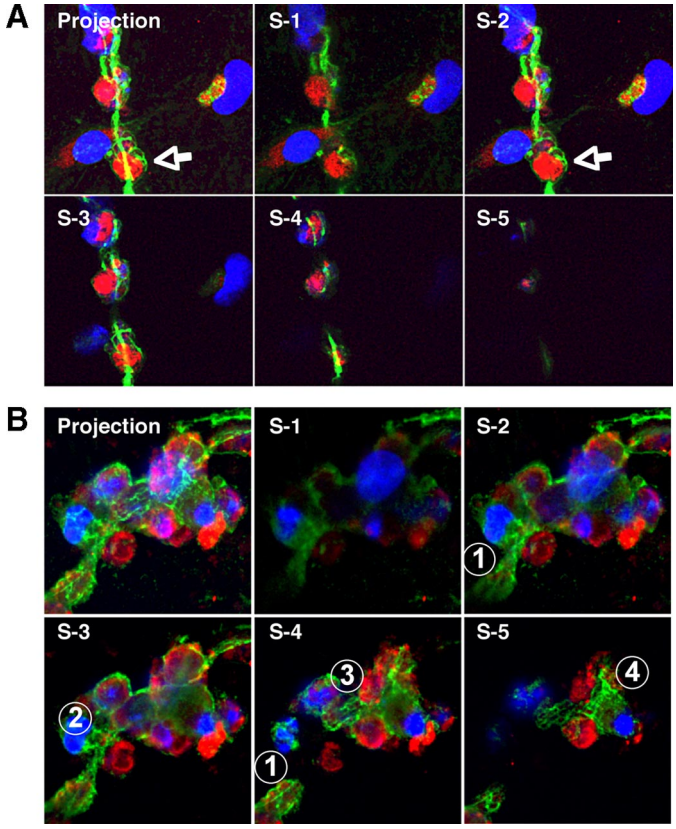

FIGURE 9. **Confocal microscopic analysis of hyaluronan cable structures and cyclin D3 in high glucose-treated RMC cultures.** *Panels A* and *B* show two enlargements of the hyaluronan cable structure and their consecutive *z*-stacks of confocal microscopic analysis from Fig. 8*A*. Note the hyaluronan structures (*green*) with closely associated, coalesced, and intertwined spots of cyclin D3 (*red*) distributed along the hyaluronan cables. See the SM1 and SM2 videos of 3-D reconstructions in the supplemental material.

(see below). These results suggest that cyclin D3 is associated with, or organizes a complex set of proteins that likely includes an activated hyaluronan synthase and C/EBPα.

Fig. 9 shows enlargements of two hyaluronan structures clustered with mesangial cells and cyclin D3. Their overall projections were dissected into the consecutive 5-μm *z* axis stacks from confocal micrographs. Clearly, hyaluronan cables were continuously extended through and between adjacent cells in a three-dimensional fashion and intertwined with cyclin D3 structures. Note that the stacks of the coalesced cyclin D3 structure indicated by the *arrow* in Fig. 9*A* do not appear to be closely associated with the adjacent cell nucleus and may, therefore, be extracellular (see Fig. 10). The sequence S-1 to S-3 in Fig. 9*A* also shows the close association of the cyclin D3-hyaluronan structure with the nucleus of cells with coalesced hyaluronan and cyclin D3. Fig. 9*B* shows the progression of the continuous hyaluronan matrix going from the *lower left cell* (indicated by 1) through what appear to be honeycomb-like arrangements that appear in three consecutive cells (indicated by 2–4) as the stack moves vertically from the culture plate surface. This is particularly apparent in *panel S-4* where the honeycomb-like structures in cells *1* and *3* are in the same plane. This lends further support for the observation with the isolated cell that shows initial hyaluronan in the perinuclear cyclin D3 structure (Fig. 8). Three-dimensional videos of Fig. 9, *A* and *B*, are shown in supplemental material, SM1 and SM2, respectively.

Cyclin D3 and Autophagy—The cyclin D3 structures in several of the cells appear to have morphological processes similar to those that occur during autophagy, a response that cells initiate when undergoing stress, notably endoplasmic reticulum (ER) stress, when unfolded proteins over-accumulate in the ER (19, 20). This process involves early formation of small aggregates of unfolded protein that are extruded from the ER and then transferred to large aggresomes located near the nucleus. The aggresomes can fuse with lysosomes that can introduce enzymes to degrade the unfolded proteins. Microtubule-associated protein 1 light chain 3 is a marker for autophagy and is characteristic of the small aggregates and aggresomes.

The experiments in Fig. 10 indicate that LC3 co-localizes with cyclin D3 in most if not all of the coalesced cyclin D3 structures. Pre-confluent, growth-arrested mesangial cell cultures were stimulated to divide in high glucose medium for 36 h. Cultures were stained for hyaluronan (*green*), cyclin D3 (*red*), and LC3 (*magenta*) before or after permeabilization with 0.4% Triton X-100 cells as described under "Experimental Procedures." Hyaluronan staining in non-permeabilized cells (Fig. 10*B*) shows extracellular hyaluronan cables between several cells, whereas cyclin D3 staining is only prominent in large extracellular structures on two cells (*arrowheads*). An enlargement of a few cells in Fig. 10*J* shows one of these structures as well as the emerging hyaluronan cables. These extracellular

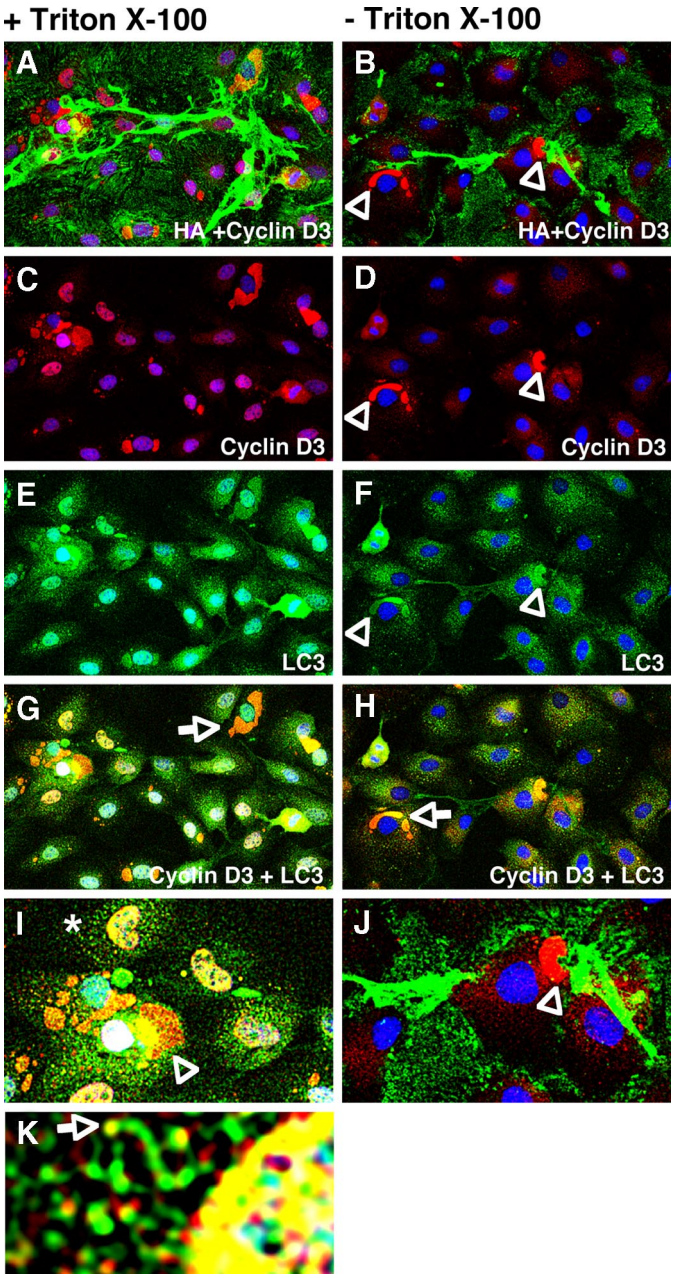

FIGURE 10. **Colocalization of cyclin D3 and LC3 in mesangial cells stimulated to divide in hyperglycemic medium.** Serum-starved mesangial cells were stimulated with 10% FBS in the presence of 25.6 mM glucose for 36 h. Cultures were treated with (*left panels*) or without (*right panels*) 0.4% Triton X-100 and stained with antisera for cyclin D3 (*red*), LC3 (*magenta* converted to *green*), hyaluronan (*HA*, *green*), and nuclei (*blue*) as described under "Experimental Procedures."

cyclin D3 structures appear similar to those described in a review of aggresomes (19). Hyaluronan staining in permeabilized cells (Fig. 10*A*) shows the continuous cable structures between and through a number of cells as observed in Fig. 8. In this case the coalesced cyclin D3 structures are now apparent in many cells, indicating that they remain intracellular closely associated with nuclei typical of aggresomes (19, 21). The difference in cyclin D3 staining before and after permeabilization is more apparent in Fig. 10, *C* and *D*, showing cyclin D3 staining alone. LC3 staining (Figs. 10, *E* and *F*, *magenta* converted to *green*) shows diffuse staining on the surface of the non-permeabilized cells with prominent staining of the same large structures that stained for cyclin D3 (Fig. 10*F*, *arrowheads*). After permeabilization (Fig. 10*E*), LC3 staining shows prominent localization above the cell nuclei in most, if not all cells, which masks the underlying nuclei. The overlay of cyclin D3 with LC3 (Fig. 10*G*) shows that they colocalize in these structures in different proportions in these cells. Furthermore, the pattern of these structures shows the same honeycomb-like organization that was observed for the cell in Fig. 8 and the hyaluronan patterns in Fig. 9. This is more apparent in the enlargement featuring several cells (Fig. 10*I*). The diffuse LC3 staining is more prominent and punctuate after permeabilization. An enlargement of a region adjacent to the honeycomb-like structure of the cell with an *asterisk* shows this pattern more prominently (Fig. 10*K*). The LC3 stain shows small spheres, sometimes in strands (*arrow*) and attached to the periphery of the honeycomb-like structure, a pattern typical of autophagic aggregates (21). Furthermore, the cyclin D3 stain shows interspersed spheres of similar size (*red*) and often colocalized with LC3 (*yellow*). The large cell (Fig. 10*I*, *arrowhead*) shows a cyclin D3 structure with interspersed LC3 staining that is similar in appearance and size to the extruded cyclin D3 structure in Fig. 10*J* (*arrowhead*) and likely represents extracellular material. Similarly, the large crescent-shaped structure in Fig. 10*G* (*arrow*) appears to be extracellular and resembles a similar structure in the non-permeabilized cell in Fig. 10*H* (*arrow*). Parallel cultures treated for 36 h in low glucose did not show significant cyclin D3 nor LC3 responses (data not shown).

Induction of Hyaluronan-mediated Monocyte Adhesion by Poly(I:C) and Tunicamycin—Previous studies have shown that treatment of smooth muscle cells with poly(I:C), which initiates responses similar to viral infection, or with tunicamycin, which initiates endoplasmic reticulum stress (also referred to as unfolded protein response), induces synthesis of the hyaluronan matrix (5, 6). Fig. 11*A* shows that preconfluent mesangial cells stimulated to divide in medium with normal, 5.6 mM glucose respond to both of these reagents by synthesis of a hyaluronan matrix (*lower panel*) that is adhesive for U937 cells (*upper panel*, *black bars*). Pretreatment of cultures with *Streptomyces* hyaluronidase before adding the U937 cells demonstrates that most of the U937 cells were bound to the hyaluronan matrices. As expected, pretreatment of poly(I:C)-treated cultures with hyaluronidase exposes vascular cell adhesion molecule cell surface receptors that are up-regulated in response to poly(I:C) and that are adherent for U937 cells (5) (compare *cross-hatched bars* for control and poly(I:C)). As expected, inhibition of protein synthesis by tunicamycin shows no increase in U937 adhesion after hyaluronidase treatment. Furthermore, in contrast to the response of dividing mesangial cells to hyperglycemic medium, cyclin D3 is decreased significantly from the control level in both the poly(I:C) and tunicamycin-treated cultures as indicated by the Western blots (Fig. 11*B*). These results indicate that the pathways that respond to poly(I:C) and tunicamycin in medium with low glucose are independent of cyclin D3 and, therefore, are distinct from that which initiates synthesis of the hyaluronan matrix by dividing mesangial cells in response to hyperglycemia.

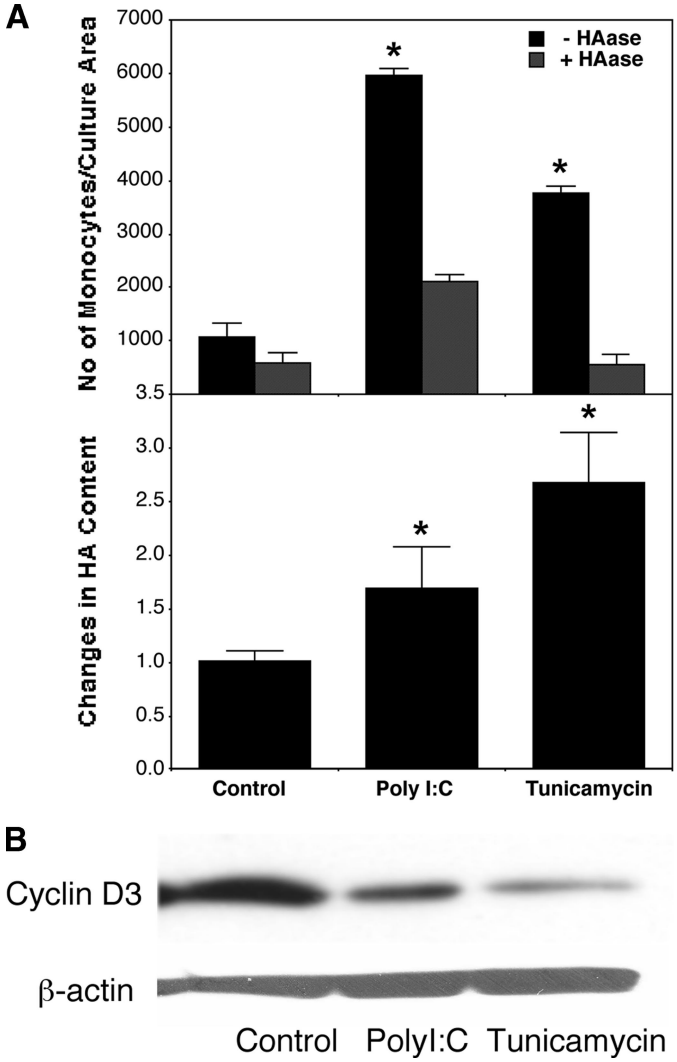

FIGURE 11. **Induction of monocyte adhesion and hyaluronan synthesis by poly(I:C) and tunicamycin independent of cyclin D3.** Serum-starved mesangial cells were stimulated with 10% FBS in 5.6 mM glucose for 48 h and then treated with or without poly(I:C) or tunicamycin for 24 h as described under "Experimental Procedures." Monocyte adhesion (*A*, *upper panel*) was measured before (*black bars*) and after (*gray bars*) digestion with *Streptomyces* hyaluronidase (*HAase*). Changes in hyaluronan contents were also determined (*A*, *lower panel*). The mean values and S.D. were calculated for three independent experiments (*, $p < 0.01$, $n = 3$). *Panel B* shows Western blots for both treatments compared with a control that was cultured in medium with 5.6 mM glucose.

Expression of Cyclin D3 and C/EBPα in Diabetic Kidney—In separate experiments we have shown that glomeruli isolated from diabetic rats 4 weeks after treatment with streptozotocin have 3–4 times as much hyaluronan as glomeruli from control rats using fluorophore-assisted carbohydrate electrophoresis procedures (data not shown). Fig. 12 shows micrographs of sections of control and 4-week diabetic kidneys. Glomeruli in sections from kidneys of control (*left panels*) and 4 week diabetic (*right panels*) animals were stained for hyaluronan (*green*) and cyclin D3 (*red*) (Fig. 12*A*) and for hyaluronan (*green*) and C/EBPα (*red*) (Fig. 12*B*). In contrast to the controls, the sections from the diabetic kidney show significant cyclin D3 and C/EBPα responses associated with a hyaluronan matrix response in the glomeruli. There are also major cyclin D3 and C/EBPα responses in the adjacent renal tubules as well as hyaluronan responses in adjacent and underlying matrices. The green in control sections is autofluorescence from extracellular matrices around the renal tubules (*upper left panels*). The cyclin D3 and C/EBPα responses in the surrounding tubular areas are striking.

DISCUSSION

Exposure of various cells, including mesangial cells, to hyperglycemia can stimulate hyaluronan synthesis (4, 22–24), but the molecular mechanisms that mediate these responses are unknown. Our previous studies have shown that quiescent, growth-arrested rat mesangial cells, stimulated to divide in a hyperglycemic level of glucose (25.6 mM), form a hyaluronan matrix that is adhesive for U937 monocytic cells. In contrast, when confluent RMC cultures were treated identically, the number of adherent monocytes in cultures treated with 25.6 mM glucose did not increase significantly beyond the number adhering to preconfluent cultures in response to 5.6 mM glucose (4). This result suggests that the response is likely to be cell growth state-dependent. In this report we investigated the effect of growth stimulation of quiescent mesangial cells in high glucose medium to identify the molecules that are essential for the hyperglycemia-induced hyaluronan synthesis. The quiescent mesangial cells require 10% FBS to re-enter the cell cycle, and they complete one mitotic cycle by ~24 h after the stimulation (11, 17). We have here shown that this concentration of serum is sufficient to reach a plateau value for induction of cell layer hyaluronan content and U937 monocyte adhesion. This confirms our previous observation that serum-stimulated cell division of quiescent cells is critical for the formation of monocyte adhesive hyaluronan matrix response to high glucose. It also suggests that the transient proliferation of mesangial cells in glomeruli *in vivo* after inducing hyperglycemia is accompanied by the synthesis of the hyaluronan matrix with subsequent recruitment of monocytes and macrophages (3, 4). The time course studies demonstrate that significant intracellular synthesis of hyaluronan is induced by the high glucose and is already apparent at 18 h, whereas significant monocyte adhesion only takes place sometime between 24 and 48 h after cells have completed a cell cycle. Therefore, the hyaluronan synthesis response actually precedes the large cyclin D3 response that also occurs between 24 and 48 h. Nevertheless, the cyclin D3 response controls the formation of the monocyte adhesive extracellular matrix because silencing cyclin D3 prevents its formation. Paradoxically, mesangial cells cultured for 72 h after silencing cyclin D3 did not show significant accumulation of hyaluronan in response to hyperglycemia, which suggests that any hyaluronan synthesized during the first cell division stage may have been degraded by the cells during the subsequent time in culture.

After completing cell division in hyperglycemic medium, mesangial cells become hypertrophic, characterized as an increase in protein content without DNA replication (25). However, the role of cell cycle progression in the high glucose induced hyaluronan synthesis response is unclear. Previous studies have shown that the activation of the CDK-cyclin complex has a pivotal role in regulating cell growth (26). Among the cyclins, the major function of cyclin D1 and cyclin D2 is to

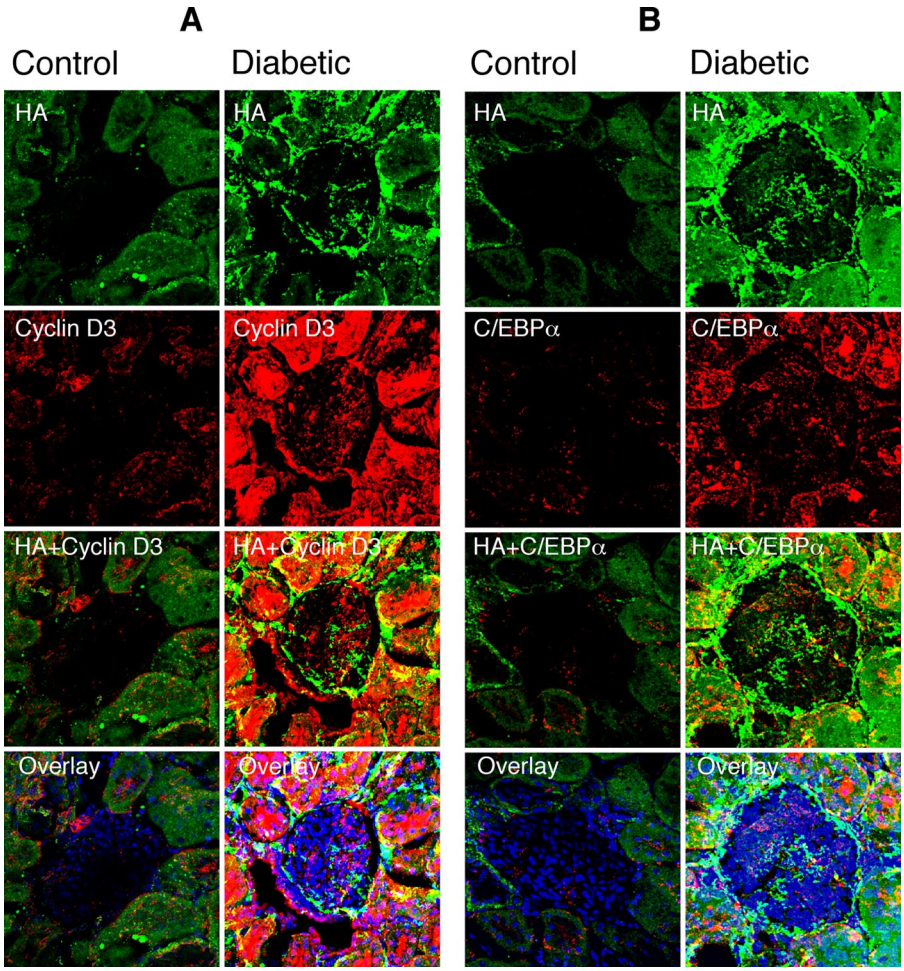

FIGURE 12. **Confocal microscopic analysis of hyaluronan, cyclin D3, and C/EBPα in sections with glomeruli and associated renal tubules.** The sections of kidneys from 4-week control and 4-week diabetic rats were stained for hyaluronan (*HA*, *green*), nuclei (*blue*), and either cyclin D3 (*red*) in *panel A* or C/EBPα (*red*) in *panel B* as described under "Experimental Procedures."

activate CDK4/CDK6 to promote proliferation (26–28). In contrast, cyclin D3 is found in the growth arrest cells and functions in cell growth arrest and differentiation (18, 29–35). This is consistent with the modest increase in cyclin D3 observed at 48 and 72 h in mesangial cell cultures stimulated to divide in low glucose medium (Fig. 4). In contrast, the large cyclin D3 increase in the mesangial cell cultures stimulated to divide in hyperglycemic medium participates in, and potentially controls an autophagic process that includes a mechanism to extrude hyaluronan into the extracellular space in cable-like structures that are adhesive for monocytes.

Our previous study (4) showed that inhibitors of protein kinase C (bisindolylmaleimide I and Gö 6976) added to hyperglycemic mesangial cell cultures at time 0, when cell division is initiated, prevent the formation of the monocyte adhesive hyaluronan matrix as measured at 72 h. A recent paper by Sakaki *et al.* (21) showed that stimulation of an immortalized hepatocyte cell line with protein kinase θ in cells subjected to ER stress initiated autophagy and that the Gö 6976 inhibitor prevented the autophagic response. Furthermore, electron micrographs in Fig. 1, *e* and *f*, of their paper showed cells with large "autophagosomes" (aggresomes) that contained fragments of ER surrounded by unstained matrix that resembles the honeycomb-like structures observed in Figs. 8–10. Hyaluronan matrices do not stain well in sections prepared for electron microscopy. This suggests that the unstained matrix observed throughout the "autophagosome" in this paper is quite possibly hyaluronan. An emerging model consistent with our data would be that a protein kinase C (PKC; likely PKCθ) is up-regulated rapidly (within the first 2 h (36) after initiating mesangial cell division in hyperglycemic medium. This in turn can activate pathways that initiate hyaluronan synthesis. Intracellular accumulation of hyaluronan could then lead to ER stress, which is considered to be central to autophagy, which then could initiate the later cyclin D3-mediated autophagic response and the formation of the monocyte adhesive hyaluronan matrix.

The growth inhibitory role of cyclin D3 has been well established in other cell systems through interaction with C/EBPα (18, 35). C/EBPα is the first protein to be identified in the family of CCAAT/enhancer-binding proteins and binds to the CCAAT motif found in several gene promoters as well as in "core homology" sequences present in certain viral enhancers (37). In young liver, cyclin D3 supports quiescence by stabilizing growth inhibitory complexes of C/EBPα with CDK2 and with Brahma protein (Brm), a transcriptional activator. In older liver, cyclin D3 and C/EBPα form complexes with Brm, Rb, and E2F4 to inhibit cell proliferation (18). Our data show that high glucose induces the formation of a complex that contains both cyclin D3 and C/EBPα between 24 and 48 h in mesangial cells after the serum stimulation in high glucose medium. This complex could have a role in inhibiting further cell growth after completion of a mitotic cycle under hyperglycemia. Indeed, high glucose inhibits cell proliferation in several cell culture models, including mesangial cells (25, 38–40).

Increased expression of C/EBPα could also have an important impact on glucose uptake by mesangial cells and its subsequent metabolism. C/EBPα is a pleiotropic transcriptional activator of adipocyte-specific genes. Overexpression of this activator in 3T3-L1 preadipocytes alone is sufficient to stimulate adipogenesis and the expression of genes responsible for insulin sensitivity, including insulin receptor (IRS-1) and Glut4, a high affinity glucose transporter, as well as the accumulation of cytoplasmic triglycerides (41, 42). Interestingly, the conversion of 3T3-L1 cells to adipocytes involves stimulating the precursor cells to divide in hyperglycemic medium. This is accompanied by the synthesis of a highly viscous hyaluronan matrix

(43). Glut4 is the major insulin-responsive glucose transporter and is primarily retained in the intracellular compartment in basal conditions. Previous studies have shown that C/EBPα has the potential to maintain the ability of insulin-stimulated Glut4 translocation to the plasma membrane (44). Thus, our observations suggest that high glucose-induced complexes with cyclin D3 and C/EBPα may have a role in influx of glucose into the cells as well as in promoting hyaluronan synthesis.

In addition, studies from Hanson and co-workers (45) show that C/EBPα is required for expression of glucokinase, an enzyme that facilitates phosphorylation of glucose to glucose 6-phosphate, the first step of glycolysis. On the other hand, excessive intracellular glucose would increase mitochondria reactive oxygen species formation, which impedes the glycolytic pathway by inhibiting glyceraldehyde-3-phosphate dehydrogenase (46). Taken together, these events would result in an overabundance of intracellular glucose and its metabolites, glucose 6-phosphate, fructose 6-phosphate, and glyceraldehyde 3-phosphate. The accumulation of these molecules inside of cells would divert the glucose into polyol, hexosamine, protein kinase C, and advanced glycation end product pathways that mediate diabetic complications in various tissues.

Immunostaining showed that cyclin D3 coalesces into large perinuclear honeycomb-like structures that are integrated with the hyaluronan matrix. These structures also contain LC3, indicative of activation of an autophagic response. The close early association of hyaluronan with these structures (Fig. 8) and the imprint of these structures in the resulting hyaluronan matrix (Fig. 9) suggest that cyclin D3 may be involved in organizing the intracellular hyaluronan synthases involved. Hyaluronan can be synthesized either on the inner side of the plasma membrane or in perinuclear locations by hyaluronan synthase enzymes that alternately add the substrates UDP-glucuronic acid and UDP-*N*-acetylglucosamine to the reducing end of the growing chain (47, 48). There are three hyaluronan synthase genes identified in mammalian cells: Has1, Has2, and Has3 (49). Serine phosphorylation by protein kinase can activate all three hyaluronan synthase isoforms, leading to increased hyaluronan production (50). One of the major functions of cyclin D3 is to activate cyclin-dependent kinases CDK4 and CDK6 (26–28). Both of these kinases belong to a large family of heterodimeric serine/threonine protein kinases. Hyperglycemia induced cyclin D3 association with both CDK4 (Fig. 4) and CDK6 (data not shown) in immunoprecipitation experiments. Thus, these results suggest that cyclin D3 could promote activation of latent, intracellular hyaluronan synthase enzymes by phosphorylation through associated CDKs, thereby initiating hyaluronan production.

We also observed increased hyaluronan matrix and expression of cyclin D3 and C/EBPα in sections of 4-week diabetic glomeruli and adjacent renal tubular cells. Indeed, the exposure to high glucose concentrations also increases hyaluronan synthesis in renal tubular cells, in renal interstitial fibroblasts, and in vascular smooth muscle cells (22–24). The primary response of cells or tissues to hyperglycemia could be to lower glucose levels by an effective mechanism through synthesis of hyaluronan. The energy cost for synthesis of a disaccharide of hyaluronan is minimal. It requires a single enzyme, and some of the metabolic cost of synthesizing the UDP-sugar precursors is recovered by the production of NADPH from the oxidation of UDP-glucose to UDP-glucuronic acid, which can be re-oxidized to NADP to yield ATP. However, the mechanism for synthesis of the hyaluronan chosen by many cells (mesangial cells, smooth muscle cells, epithelial cells) is one that produces a hyaluronan-enriched matrix, but this matrix has a structure that is recognized by inflammatory cells and has a major role in most, if not all inflammatory processes. Thus, the broader implications of cyclin D3-mediated responses may begin to clarify mechanisms involved in many diabetic pathologies.

REFERENCES

1. Wolf, G., and Ziyadeh, F. N. (1999) *Kidney Int.* **56,** 393–405
2. Young, B., Johnson, R., Alpers, C., Eng, E., Floege, J., and Couser, W. (1992) *J. Am. Soc. Nephrol.* **3,** 770 (Abstr. 73P)
3. Young, B. A., Johnson, R. J., Alpers, C. E., Eng, E., Gordon, K., Floege, J., Couser, W. G., and Seidel, K. (1995) *Kidney Int.* **47,** 935–944
4. Wang, A., and Hascall, V. C. (2004) *J. Biol. Chem.* **279,** 10279–10285
5. de La Motte, C. A., Hascall, V. C., Calabro, A., Yen-Lieberman, B., and Strong, S. A. (1999) *J. Biol. Chem.* **274,** 30747–30755
6. Majors, A. K., Austin, R. C., de la Motte, C. A., Pyeritz, R. E., Hascall, V. C., Kessler, S. P., Sen, G., and Strong, S. A. (2003) *J. Biol. Chem.* **278,** 47223–47231
7. Simonson, M. S., and Dunn, M. J. (1990) *Methods Enzymol.* **187,** 544–553
8. Templeton, D. M. (1990) *J. Biol. Chem.* **265,** 21764–21770
9. Hegele, R. G., Behar, M., Katz, A., and Silverman, M. (1989) *Clin. Investig. Med.* **12,** 181–186
10. Mené, P., Simonson, M. S., and Dunn, M. J. (1989) *Physiol. Rev.* **69,** 1347–1424
11. Wang, A., Fan, M. Y., and Templeton, D. M. (1994) *J. Cell. Physiol.* **159,** 295–310
12. Lauer, M. E., Hascall, V. C., and Wang, A. (2007) *J. Biol. Chem.* **282,** 843–852
13. de la Motte, C. A., Hascall, V. C., Drazba, J., Bandyopadhyay, S. K., and Strong, S. A. (2003) *Am. J. Pathol.* **163,** 121–133
14. Evanko, S. P., and Wight, T. N. (1999) *J. Histochem. Cytochem.* **47,** 1331–1342
15. Calabro, A., Benavides, M., Tammi, M., Hascall, V. C., and Midura, R. J. (2000) *Glycobiology* **10,** 273–281
16. Calabro, A., Hascall, V. C., and Midura, R. J. (2000) *Glycobiology* **10,** 283–293
17. Wang, A., and Templeton, D. M. (1996) *Kidney Int.* **49,** 437–448
18. Wang, G. L., Shi, X., Salisbury, E., Sun, Y., Albrecht, J. H., Smith, R. G., and Timchenko, N. A. (2006) *Mol. Cell. Biol.* **26,** 2570–2582
19. Garcia-Mata, R., Gao, Y. S., and Sztul, E. (2002) *Traffic* **3,** 388–396
20. Sakaki, K., and Kaufman, R. J. (2008) *Autophagy* **4,** 841–843
21. Sakaki, K., Wu, J., and Kaufman, R. J. (2008) *J. Biol. Chem.* **283,** 15370–15380
22. Erikstrup, C., Pedersen, L. M., Heickendorff, L., Ledet, T., and Rasmussen, L. M. (2001) *Eur. J. Endocrinol.* **145,** 193–198
23. Takeda, M., Babazono, T., Nitta, K., and Iwamoto, Y. (2001) *Metabolism* **50,** 789–794
24. Jones, S., Jones, S., and Phillips, A. O. (2001) *Kidney Int.* **59,** 1739–1749
25. Wolf, G., Schroeder, R., Zahner, G., Stahl, R. A., and Shankland, S. J. (2001) *Am. J. Pathol.* **158,** 1091–1100
26. Malumbres, M., and Barbacid, M. (2005) *Trends Biochem. Sci.* **30,** 630–641
27. Blain, S. W. (2008) *Cell Cycle* **7,** 892–898
28. Bloom, J., and Cross, F. R. (2007) *Nat. Rev. Mol. Cell Biol.* **8,** 149–160
29. Bartkova, J., Lukas, J., Strauss, M., and Bartek, J. (1998) *Oncogene* **17,** 1027–1037
30. Doglioni, C., Chiarelli, C., Macri, E., Dei Tos, A. P., Meggiolaro, E., Dalla Palma, P., and Barbareschi, M. (1998) *J. Pathol.* **185,** 159–166
31. Cenciarelli, C., De Santa, F., Puri, P. L., Mattei, E., Ricci, L., Bucci, F.,

Felsani, A., and Caruso, M. (1999) *Mol. Cell. Biol.* **19,** 5203–5217
32. de la Serna, I. L., Roy, K., Carlson, K. A., and Imbalzano, A. N. (2001) *J. Biol. Chem.* **276,** 41486–41491
33. Reichert, M., and Eick, D. (1999) *Oncogene* **18,** 459–466
34. Rickheim, D. G., Nelsen, C. J., Fassett, J. T., Timchenko, N. A., Hansen, L. K., and Albrecht, J. H. (2002) *Hepatology* **36,** 30–38
35. Wang, G. L., Shi, X., Salisbury, E., and Timchenko, N. A. (2008) *Exp. Cell Res.* **314,** 1626–1639
36. Xia, L., Wang, H., Munk, S., Kwan, J., Goldberg, H. J., Fantus, I. G., and Whiteside, C. I. (2008) *Am. J. Physiol. Renal Physiol.* **295,** F1705–1714
37. Ramji, D. P., and Foka, P. (2002) *Biochem. J.* **365,** 561–575
38. Hayashi, J. N., Ito, H., Kanayasu, T., Asuwa, N., Morita, I., Ishii, T., and Murota, S. (1991) *Virchows Arch. B Cell Pathol. Incl. Mol. Pathol.* **60,** 245–252
39. Cosio, F. G. (1995) *J. Am. Soc. Nephrol.* **5,** 1600–1609
40. Zheng, X. L., Yuan, S. G., and Peng, D. Q. (2007) *Diabetologia* **50,** 881–890
41. MacDougald, O. A., and Lane, M. D. (1995) *Annu. Rev. Biochem.* **64,** 345–373
42. Rosen, E. D. (2005) *Prostaglandins Leukot. Essent. Fatty Acids* **73,** 31–34
43. Calvo, J. C., Gandjbakhche, A. H., Nossal, R., Hascall, V. C., and Yanagishita, M. (1993) *Arch. Biochem. Biophys.* **302,** 468–475
44. Fujimoto, M., Masuzaki, H., Yamamoto, Y., Norisada, N., Imori, M., Yoshimoto, M., Tomita, T., Tanaka, T., Okazawa, K., Fujikura, J., Chusho, H., Ebihara, K., Hayashi, T., Hosoda, K., Inoue, G., and Nakao, K. (2005) *Biochim. Biophys. Acta* **1745,** 38–47
45. Yang, J., Croniger, C. M., Lekstrom-Himes, J., Zhang, P., Fenyus, M., Tenen, D. G., Darlington, G. J., and Hanson, R. W. (2005) *J. Biol. Chem.* **280,** 38689–38699
46. Brownlee, M. (2001) *Nature* **414,** 813–820
47. Toole, B. P. (2000) in *Proteoglycans*: *Structure*, *Biology*, *and Molecular Interactions* (Iozzo, R. V., ed) pp. 61–92, Marcel Dekker, Inc., New York
48. Hascall, V. C., Majors, A. K., De La Motte, C. A., Evanko, S. P., Wang, A., Drazba, J. A., Strong, S. A., and Wight, T. N. (2004) *Biochim. Biophys. Acta* **1673,** 3–12
49. Weigel, P. H., Hascall, V. C., and Tammi, M. (1997) *J. Biol. Chem.* **272,** 13997–14000
50. Bourguignon, L. Y., Gilad, E., and Peyrollier, K. (2007) *J. Biol. Chem.* **282,** 19426–19441